OPEN ACCESS
JOURNAL OF ADVANCED DIELECTRICS
Vol. 13, No. 6 (2023) 2340006 (11 pages)

DOI: 10.1142/S2010135X23400064

Structures, dielectric properties and AC impedance characteristics of $BiFeO_3$–$BaTiO_3$ high-temperature lead-free piezoceramics synthesized by the hydrothermal method*

Shuangchi Li[†], Fang Wang[†], Lanxin Tang[†], Daniel Q. Tan[‡] and Yu Chen[†,§]
[†]*School of Mechanical Engineering, Chengdu University*
Chengdu 610106, P. R. China
[‡]*Department of Materials Science and Engineering*
Guangdong Technion-Israel Institute of Technology
Shantou 515063, P. R. China
[§]chenyu01@cdu.edu.cn

Received 16 September 2023; Revised 3 November 2023; Accepted 7 November 2023; Published 7 December 2023

Among the lead-free piezoceramics, $(1-x)BiFeO_3 - xBaTiO_3$ (BF-BT) is considered a promising candidate for high-temperature piezoelectric materials owing to its high Curie temperature ($T_C > 400^\circ$C) and good electromechanical properties. In this work, the hydrothermal synthesis method was used to prepare the precursor powders of $BiFeO_3$ and $BaTiO_3$, and then the mixed powder compacts with the chemical composition of 0.7BF–0.3BT were sintered under pressureless conditions. The influence of the hydrothermal reaction times (12–24 h) of $BiFeO_3$ on the structures and electric properties of the sintered ceramics was instigated. First, all the samples synthesized with the tetragonal $BaTiO_3$ and $BiFeO_3$ powders were identified with relatively stable dielectric properties. As the hydrothermal reaction time to synthesize $BiFeO_3$ increased, the dielectric properties as well as the temperature stability of the $0.7BiFeO_3$–$0.3BaTiO_3$ ceramics also improved. At the condition of a hydrothermal reaction time of 24 h, the sample obtained possesses both the lowest temperature coefficient of dielectric constant ($Tk_\varepsilon = 1.53 \times 10^{-2}/^\circ$C between RT and 300°C) and the highest Curie temperature ($T_C = 471^\circ$C at 100 kHz). Moreover, at high temperatures, it exhibits a higher AC impedance than others. The calculating result based on the resistive constant-phase-element model (R-CPE) circuit model showed that the grain boundary of the 0.7BF–0.3BT ceramics contributes more resistance to the conductivity at high temperatures. In summary, the hydrothermal reaction proved to be a useful way that achieves the preparation of single-phase 0.7BF–0.3BT ceramics with improved electrical properties.

Keywords: Hydrothermal reaction; $BiFeO_3$; $BaTiO_3$; dielectrical properties; AC impedance.

1. Introduction

Bismuth ferrite ($BiFeO_3$) is a typical single-phase multiferroic material at room temperature. It has a Curie temperature (T_C) of approximately 1103 K and a Neel temperature of around 643 K.[1–3] It is one of the few multiferroic materials exhibiting both ferroelectric and antiferromagnetic ordering at room temperature. Structurally, $BiFeO_3$ adopts a distorted rhombohedral perovskite structure, belonging to the R3c space group. In this structure, Bi atoms occupy the vertex positions, Fe ions are located at the centers of the iron oxide octahedra and O atoms occupy the face-centered positions.[4–7] However, the synthesis of $BiFeO_3$ often results in the formation of impurities due to the volatility of bismuth and the fluctuation of iron oxidation states. This leads to higher leakage current, lower resistivity and smaller dielectric constant in $BiFeO_3$ samples, making it difficult to obtain saturated hysteresis loops at room temperature. Therefore, some researchers have incorporated $BaTiO_3$ into $BiFeO_3$ to suppress the formation of impurities and stabilize the $BiFeO_3$ structure.[3,8,9]

Similar to other lead-based piezoelectric systems such as KNN, $BiFeO_3$–$BaTiO_3$ (BF-BT) exhibits excellent piezoelectric and ferroelectric properties when the system is near the morphotropic phase boundary (MPB).[10–12] However, during the sintering process of BF-BT ceramics, phenomena such as the volatilization of Bi_2O_3 and the variable valence of Fe^{3+} contribute to a higher concentration of defect ions in the ceramic samples.[13–15] As a result, this process leads to higher dielectric loss ($\tan\delta$), poorer ferroelectric properties and lower piezoelectric performance.[9,13,16,17] Additionally, when the concentration of defect ions in the ceramic samples reaches a certain level, it can cause significant leakage current during the polarization process, making it difficult to achieve proper polarization of the ceramic samples.[2,18–21]

In the BF-BT ceramic system, the issues of low ceramic resistance, significant leakage current due to the volatilization

*This paper was originally submitted to the Special Issue on Applications of Ferroelectric Materials in Environment and Energy Fields by Yanmin Jia, Hong Liu and Yu Chen.

§Corresponding author.

of Bi_2O_3 and variable valence of Fe^{3+}, and difficulty in polarization have been addressed by several approaches. Leontsev *et al.* doped BF-BT ceramics with MnO_2, which increased the resistance from $2.7 \times 10^7\,\Omega \cdot m$ undoped to $7.6 \times 10^{12}\,\Omega \cdot m$. Furthermore, the d_{33} of the ceramic system increased from $47\,pC{\cdot}N^{-1}$ undoped to $116\,pC{\cdot}N^{-1}$. Zhou *et al.* found that substituting Bi^{3+} at the *A*-site with La^{3+} in $0.71BF - 0.29BT + 0.6\%\ MnO_2$ (0.6% mass fraction) effectively improved the ferroelectric and piezoelectric properties of the ceramic samples.[10,11,15,22,23] When the substitution amount of La^{3+} was 0.02 mol, the ceramic samples exhibited excellent piezoelectric performance with $d_{33} = 168\,pC{\cdot}N^{-1}$. Qin *et al.* analyzed the influence of furnace cooling and water quenching on the properties of 0.67BF–0.33BT ceramics. They found that the water-quenched samples exhibited saturated hysteresis loops, while the furnace-cooled samples displayed relatively saturated hysteresis loops.[14,24,25]

Although the methods mentioned above can improve the insulation and piezoelectric performance of BF-BT ceramics, these methods are complex, and it is difficult to accurately control the composition and phase structure during high-temperature sintering, which hinders industrial production and application.[26–28] Therefore, in BF-BT ceramics, how to achieve high insulation and high piezoelectric performance through process adjustment has become the focus of our attention.

In this study, the preparation of BF-BT ceramics without doping with additional components or sintering them under specific atmospheres was explored. The approach involved hydrothermal synthesis to separately prepare precursor powders of $BiFeO_3$ and $BaTiO_3$, followed by sintering to fabricate BF-BT ceramics. The study also included analysis of the phase structure, microstructure, chemical state, dielectric relaxation behavior and high-temperature impedance behavior of the samples.

2. Experimental Details

2.1. *Preparation of samples*

First, the precursor powders of $BiFeO_3$ and $BaTiO_3$ were prepared separately by using the hydrothermal reaction process as shown in Fig. 1. Second, these two kinds of powders obtained were weighted and mixed according to the molar ratio of 7:3, and then ball-milled, dried, granulated and pressed into circular discs (green bodies) with a diameter of 10 mm. After removing the adhesive, these discs were sintered at 1000°C in air for 2 h to obtain the polycrystalline ceramics. In this experiment, the 0.7BF–0.3BT ceramics prepared by the $BiFeO_3$ precursors with hydrothermal reaction times of 12, 16, 20 and 24 h were abbreviated as the samples 0.7BF–0.3BT-1, 0.7BF–0.3BT-2,0.7BF–0.3BT-3 and 0.7BF–0.3BT-4, respectively.

2.2. *Characterization of samples*

The composition and crystal structure of the samples were determined using an X-ray diffractometer (DX-2700B, DDHY, China). The surface microstructure of the samples was observed by using a scanning electron microscope (SEM) (Quanta FEG 250, FEI, USA). The surface chemical composition and elemental valence of the powder were characterized by X-ray photoelectron spectroscopy (XPS). The dielectric properties of the samples from room temperature to 560°C were measured using an LCR meter (TH2829A, Tonghui Electronics, China) associated with the furnace, and the AC impedance characteristics of the samples from 360°C to 450°C were measured.

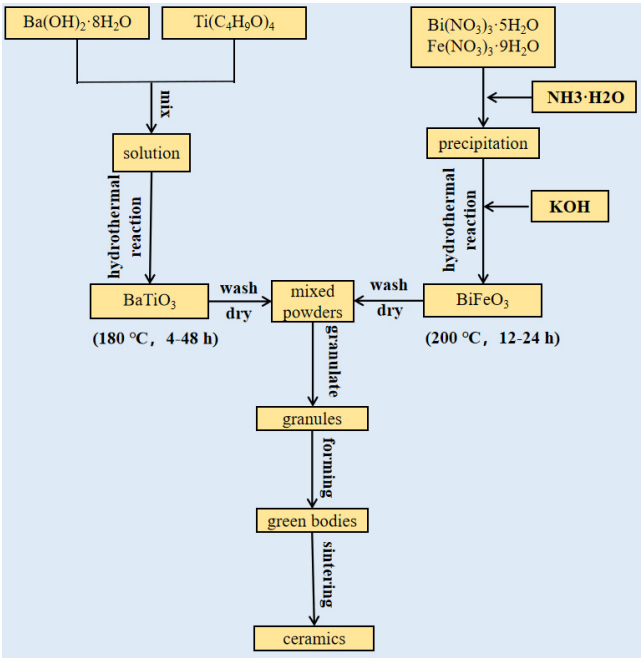

Fig. 1. Process flow for preparing the 0.7BF–0.3BT ceramics through the hydrothermal reaction method.

3. Results and Discussion

3.1. *Phase structure*

Figure 2(a) shows the XRD spectrum of $BaTiO_3$ precursor synthesized with different hydrothermal reaction times. The major diffraction peaks match with the standard card of $BaTiO_3$ (PDF#79-2263). The fixed molar ratio of Ba^{2+} to Ti^{4+} was 2:1 under highly alkaline conditions. The effect of reaction time on the preparation of tetragonal phase $BaTiO_3$ crystals was investigated and concluded that tetragonal phase barium titanate can be synthesized when the reaction temperature is 180°C and the reaction time exceeds 24 h. When the reaction temperature is 180°C and the reaction time is 18 or 24 h, the reaction is incomplete leading to the presence of Ti in the products. Tetragonal phase barium titanate with high content can be obtained when the reaction temperature exceeds 180°C and the reaction time exceeds 48 h.

Figure 2(b) shows the XRD spectrum of $BiFeO_3$ precursor synthesized with different hydrothermal reaction times.

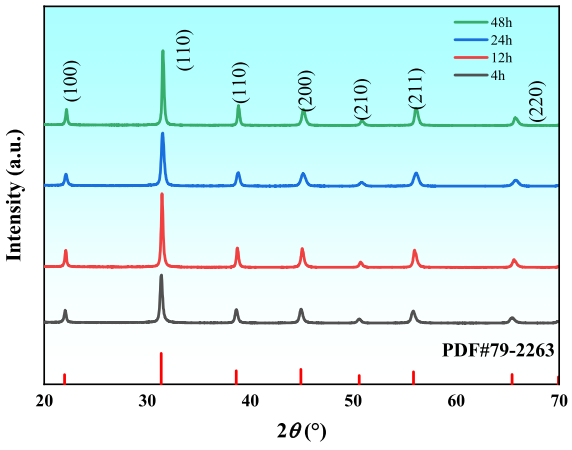

(a)

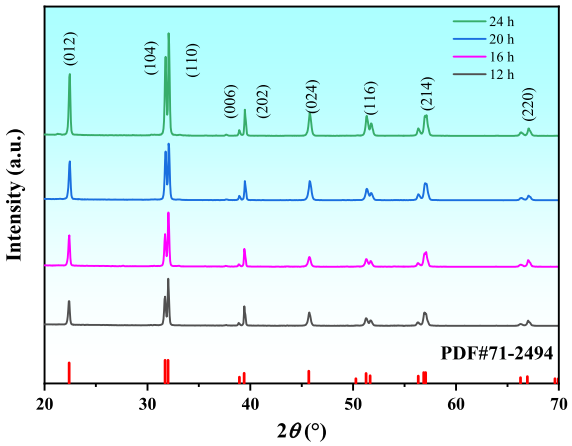

(b)

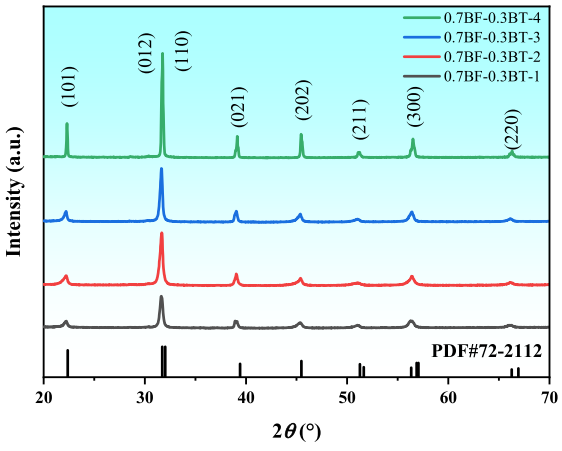

(c)

Fig. 2. XRD patterns of the samples synthesized in the experiment: (a) $BaTiO_3$ precursor, (b) $BiFeO_3$ precursor, (c) 0.7BF–0.3BT ceramics.

The crystal structure of $BiFeO_3$ belongs to the cubic phase. Single-phase $BiFeO_3$ powders can be synthesized at reaction temperatures above 140°C. The $BiFeO_3$ powders were prepared by a hydrothermal reaction at temperature of 200°C, and the intensity of the diffraction peaks increased with increasing reaction time.

Under the condition of 1000°C and 2 h, $BaTiO_3$ precursor prepared under 180°C and 48 h condition and $BiFeO_3$ precursor prepared under different reaction conditions were sintered to form BF-BT-based piezoelectric ceramics. The XRD spectrum of the sample obtained under this condition is shown in Fig. 2(c). The main phase of all samples is a perovskite structure with tetragonal symmetry, and there is no secondary phase, indicating that the BF-BT sintered from the precursor prepared by hydrothermal method forms a stable perovskite solid solution. The main diffraction peaks of BF-BT match the standard card of BF-BT (PDF #72-2112).

Figures 3(a)–3(d) represent the XRD diffraction patterns and structure refinement of the 0.7BF–0.3BT ceramics. By refining these XRD curves, it was determined that all samples contain a coexistence of trigonal and tetragonal phases, with the space group of *R*3*m* and *P*4*mm*, respectively. Moreover, as the reaction time of $BiFeO_3$ precursor increases, the content of the tetragonal phase in the samples gradually increases. Table 1 shows the lattice parameters and phase distribution of all refined samples. When the reaction time is 24 h, the content ratio of trigonal phase to cubic phase in the 0.7BF–0.3BT ceramic is approximately 7:3.

3.2. *Microscopic morphology*

Figure 4 shows the SEM images of the surface morphology of 0.7BF–0.3BT ceramic samples after thermal etching treatment, and the statistical distribution of grain sizes of these samples synthesized with different hydrothermal reaction times is shown in the inset. It can be seen from these images that as the reaction time of $BiFeO_3$ precursor increases, the ceramic grains grow gradually and become more and more rounded. Meanwhile, the grain boundaries become more and more distinct. By comparing the XRD spectra of $BiFeO_3$ precursor, it can be noted that the intensity of the diffraction peaks enhances as the reaction time increases. It can be inferred that with prolonged reaction time, the reduction in impurities and the increase in purity of the $BiFeO_3$ sample result in finer powder, promoting particle growth and leading to more complete nucleation of 0.7BF–0.3BT.

3.3. *Chemical compositions*

XPS was used to characterize the surface chemical composition and oxidation states of $BiFeO_3$ and $BaTiO_3$ powders. The XPS spectra of $BiFeO_3$ and $BaTiO_3$ precursor are shown below. The binding energy was charge-corrected using the C 1*s* peak at 284.8 eV.[29,30]

Figure 5(a) shows the XPS spectrum of $BaTiO_3$ precursor, and it indicates the presence of Ba, Ti and O elements on the material surface. The oxidation states and electronic environments of the elements were determined through XPS

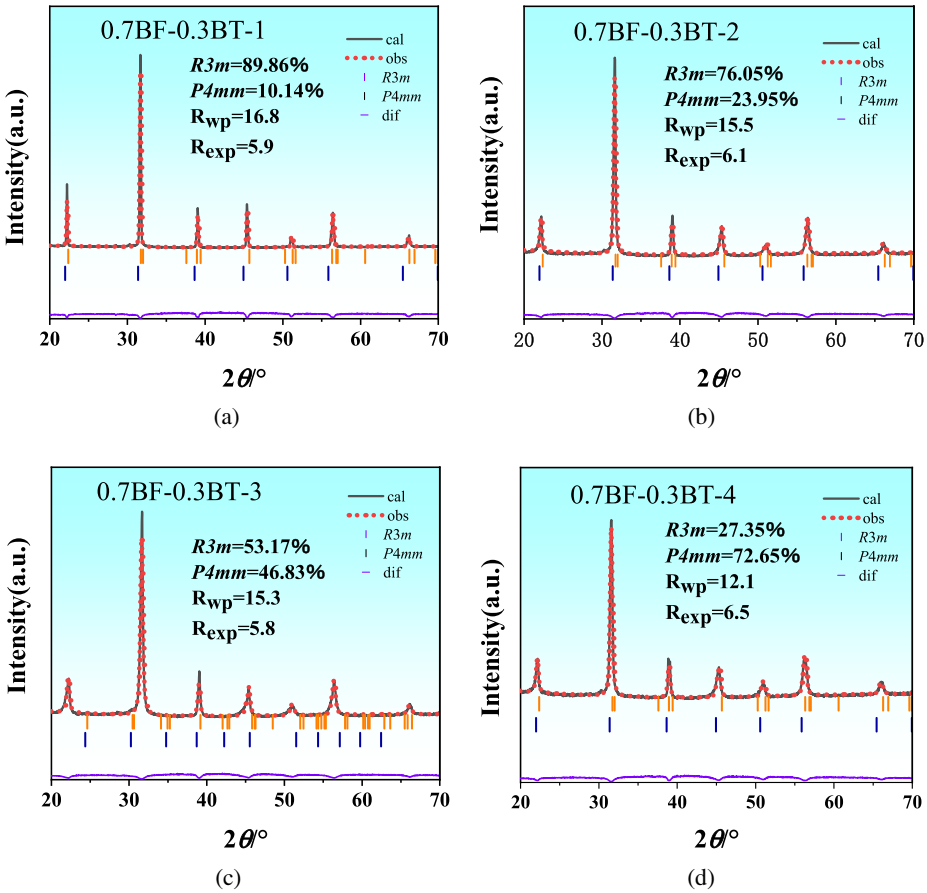

Fig. 3. Rietveld refinement of XRD patterns of the 0.7BF–0.3BT ceramics.

Table 1. Lattice parameters of the 0.7BF–0.3BT ceramics.

	Trigonal phase (*R*3*m*)			Tetragonal phase (*P*4*mm*)		
Samples	*a* (Å)	*b* (Å)	*c* (Å)	*a* (Å)	*c* (Å)	*c*/*a*
0.7BF–0.3BT–1	5.6468	5.6468	13.8857	3.9934	3.9934	2.459
0.7BF–0.3BT–2	5.6595	5.6595	13.8829	3.9961	3.9961	2.453
0.7BF–0.3BT–3	5.6419	5.6419	13.8906	3.9972	3.9972	2.462
0.7BF–0.3BT–4	5.6468	5.6468	13.8881	3.9999	3.9999	2.459

measurements. Figure 5(b) shows the narrow scan O 1*s* XPS spectrum. The two peaks at 529.25 and 530.95 eV were assigned to the lattice oxygen (Ti–O bond) and hydroxyl or absorbed oxygen in the synthesized $BaTiO_3$. Figure 5(c) shows the high-resolution Ba 3*d* XPS spectrum of $BaTiO_3$, and the two peaks at 793.65 and 778.35 eV were attributed to the splitting of the ba3$d_{3/2}$ and Ba3$d_{5/2}$ spin states, respectively. Figure 5(d) shows the narrow scan Ti 2*p* XPS spectrum, and the two peaks at 457.95 and 463.45 eV were caused by the splitting of the Ti $2p_{3/2}$ and Ti $2p_{1/2}$ spin states, respectively. The binding energy of Ti $2p_{3/2}$ was 457.95 eV, which was blue-shifted compared to the reported value of $BaTiO_3$ bulk. The decrease in binding energy was mainly due to the formation of Ti^{3+} defects. In order to balance the oxygen vacancies, some Ti^{4+} in $BaTiO_3$ was converted to Ti^{3+}.

XPS spectrum of $BiFeO_3$ precursor is shown in Fig. 6. From the XPS results, it can be concluded that there are three elements, Bi, Fe and O, on the surface of the material. The main peaks can be attributed to Bi 4*f*, Bi 4*d*, Bi 5*d*, O 1*s* and C1*s* core levels, while weak peaks can be attributed to Fe 2*p* and Bi 4*s*. Figure 6(b) shows the O 1*s* XPS spectrum. In O 1*s*, the binding energies appear at 530.2, 532.1 and 533.4 eV, respectively, corresponding to lattice oxygen, chemisorbed oxygen, and physically adsorbed oxygen. Figure 6(c) is the Fe 2*p* XPS spectrum. The double peaks at binding energies of 711.0 and 724.6 eV, respectively, correspond to the Fe $2p_{3/2}$ and Fe $2p_{1/2}$ core levels split by spin-orbit coupling, where the spin-orbit splitting energy of Fe $2p_{3/2}$ and Fe $2p_{1/2}$ is 13.6 eV, consistent with the literature value for Fe^{3+}. In addition, a satellite peak appears at 719.0 eV, between Fe $2p_{3/2}$ and Fe $2p_{1/2}$, which is 8 eV higher in binding energy than Fe $2p_{3/2}$, further confirming the presence of Fe^{3+} oxidation state in the prepared $BiFeO_3$ sample. Figure 6(d) shows the Bi 4*f* XPS spectrum. The two peak positions of the Bi 4*f* core level spectrum are at 158.5 and 163.9 eV, and the spin-orbit splitting energy is 5.4 eV, indicating the presence of Bi^{3+}.[27,29]

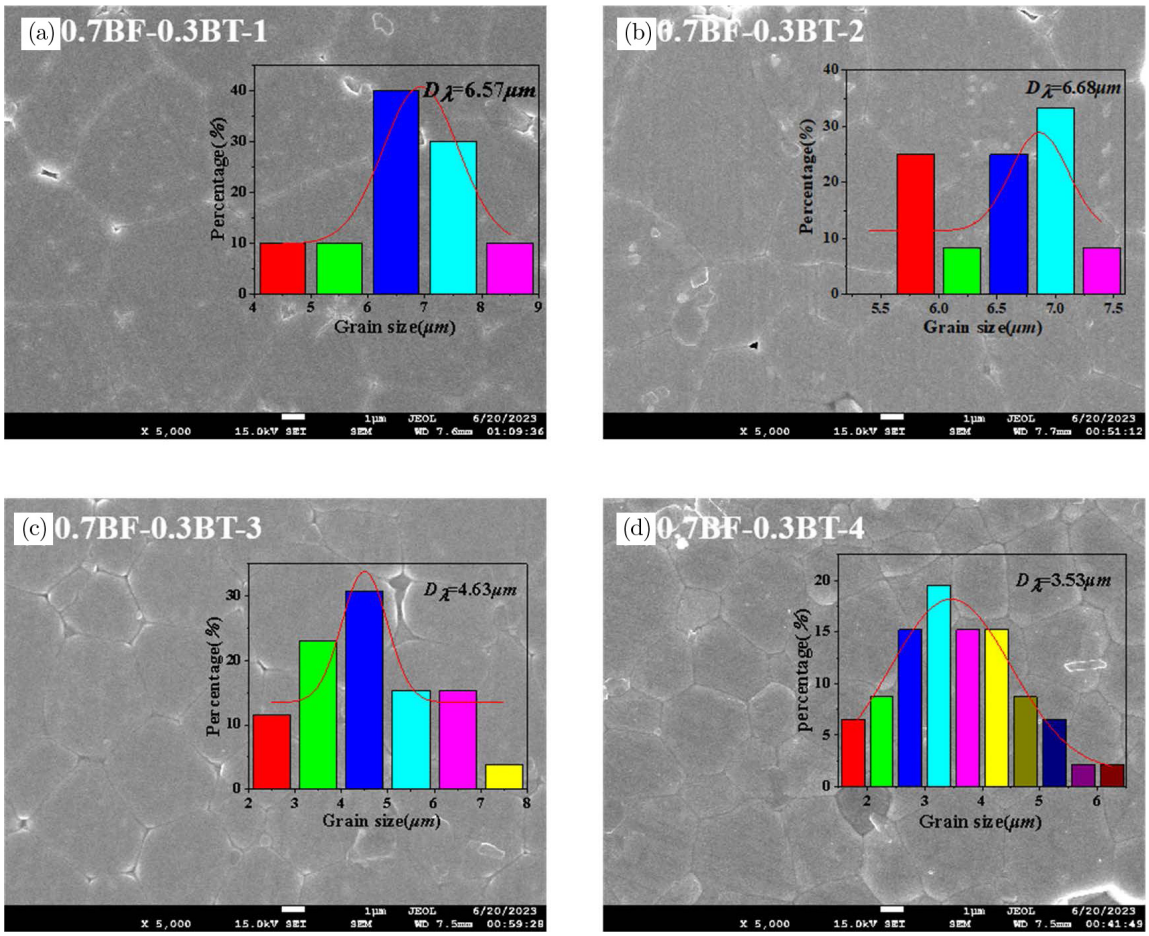

Fig. 4. SEM micro-images of the 0.7BF–0.3BT ceramics after thermal etching treatment.

3.4. *Dielectric properties*

Figures 7(a)–7(d) show the relative dielectric constant (ε_r) and dielectric loss tangent ($\tan\delta$) of the 0.7BF–0.3BT ceramics as a function of temperature. As can be seen from Fig. 7, the dielectric constant of BF-BT ceramic gradually increases with the increase of temperature, but decreases after reaching the phase transition temperature (T_m) from ferroelectric to paraelectric phase. Due to the ferroelectric to paraelectric phase transition, all samples exhibit a common dielectric peak at 400–500°C, indicating that the T_C value of the samples is within this temperature range. With the increase of $BiFeO_3$ precursor reaction time, the T_C value also exhibits a slight upward trend, suggesting that the crystallinity of the powder is improved, leading to the slight increase of T_C after sintering. It can be concluded that BF-BT ceramics synthesized by hydrothermal method from $BiFeO_3$ and $BaTiO_3$ also exhibit relatively stable performance.

It can be seen that from Fig. 7, before 200°C, the change in dielectric loss ($\tan\delta$) of the 0.7BF–0.3BT ceramics prepared with different $BiFeO_3$ precursor reaction times is not significant. However, as the temperature increases to 200°C, $\tan\delta$ increases rapidly. This phenomenon is due to the fact that at higher temperatures, the free movement of carriers is induced such as thermally activated space charge conduction. It can also be observed that the lower the frequency, the faster the $\tan\delta$ value increases, and in this process, the DC conductivity begins to dominate the entire dielectric response process. In addition, the dielectric loss of all samples at different frequencies also exhibits obvious diffuse phase transition characteristics, that is, with the increase of frequency, the maximum value of dielectric loss also moves towards higher temperatures.

In addition, from the graph, it can be seen that above the maximum dielectric constant corresponding to the phase transition temperature T_m, the dielectric and loss peaks of the ceramics move towards higher temperatures with increasing testing frequency. As the frequency increases, the intensity of the phase transition peak gradually decreases, and the width of the phase transition peak increases. Moreover, there is frequency dispersion of the phase transition peak towards higher temperatures with increasing frequency, and at each frequency, the dielectric constant peak exhibits a significant broadening feature, indicating that all the samples exhibit diffused phase transition behavior.

Unlike normal ferroelectrics, the relationship between the dielectric constant and temperature in relaxor ferroelectrics

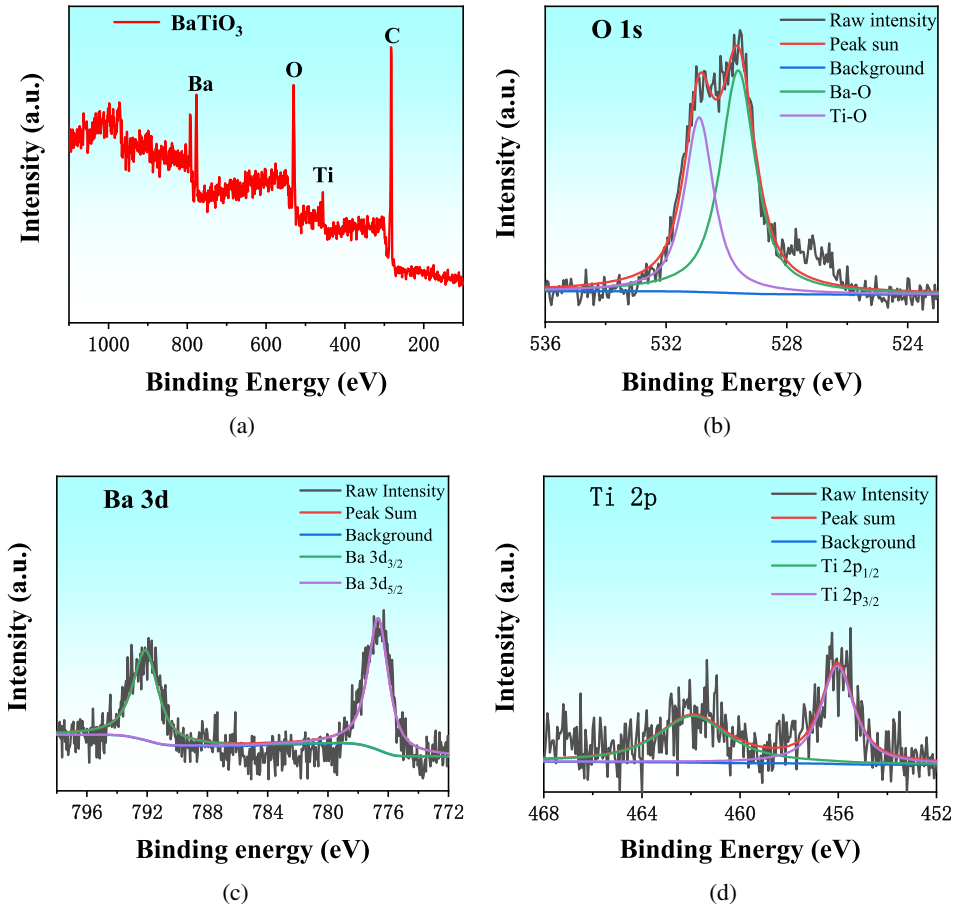

Fig. 5. (a) XPS spectrum of the $BaTiO_3$ precursor synthesized with hydrothermal reaction time of 48 h, (b) O 1*s*, (c) Ba 3*d*, (d) Ti 2*p*.

does not follow Curie–Weiss law, but it obeys a modified Curie–Weiss equation called the UN equation.[31]

$$(1/\varepsilon_r - 1/\varepsilon_m) = (T - T_m)^{\gamma}/C. \quad (1)$$

In the UN equation mentioned earlier, ε_m is the maximum dielectric constant, ε_r is the relative dielectric constant at temperature T, T_m is the temperature corresponding to the maximum dielectric constant, C is the Curie constant, and γ is the diffuse factor. By fitting the experimental data to the equation, the value of γ can be obtained. Usually, $\gamma = 1$ indicates that the material is a normal ferroelectric material, $1 < \gamma < 2$ represents that the material belongs to relaxor ferroelectrics, and $\gamma = 2$ represents the ideal relaxor ferroelectric. Figure 7(e) depicts the relationship between $\ln(1/\varepsilon_r - 1/\varepsilon_m)$ and $\ln(T - T_m)$ of the 0.7BF–0.3BT ceramics at a frequency of 100 kHz. The γ values of all the samples are larger than 1.7, indicating the 0.7BF–0.3BT ceramics are close to the ideal relaxor ferroelectric material. In addition, a slight increase in γ values occurred in 0.7BF–0.3BT–4 (Fig. 7(e)), which may be related to a significant decrease in its grain size.

Figure 8 shows the dielectric properties of the 0.7BF–0.3BT ceramics as a function of the reaction time of $BiFeO_3$ (at 100 kHz). The data obtained from the graph indicate that as the reaction time of $BiFeO_3$ precursor increases, the dielectric constant (ε_r), dielectric loss ($\tan\delta$) and phase transition temperature (T_m) all display an upward trend. Notably, both the dielectric constant and phase transition temperature exhibit significant improvements, whereas the variation range of the dielectric loss remains relatively small. This suggests that the crystallization of the powder is enhanced with a longer reaction time of $BiFeO_3$ precursor.

In order to investigate the temperature dependence of the dielectric constant of 0.7BF–0.3BT ceramics, we introduce the concept of the temperature coefficient of dielectric constant (Tk_ε), which represents the relative rate of change of the dielectric constant for each 1°C increase in temperature within a certain temperature range. Therefore, Tk_ε is used to assess the temperature stability of the dielectric properties of 0.7BF–0.3BT ceramics. The calculation formula is shown in the following equation:

$$Tk_\varepsilon = \frac{\varepsilon_T - \varepsilon_{T0}}{\varepsilon_{T0}(T - T_0)}, \quad (2)$$

where ε_T represents the dielectric constant at temperature (T) and ε_{T0} represents the dielectric constant at room temperature (T_0). From Fig. 8, the trend graphs of T_C and Tk_ε for the 0.7BF–0.3BT ceramics with varying concentration can be

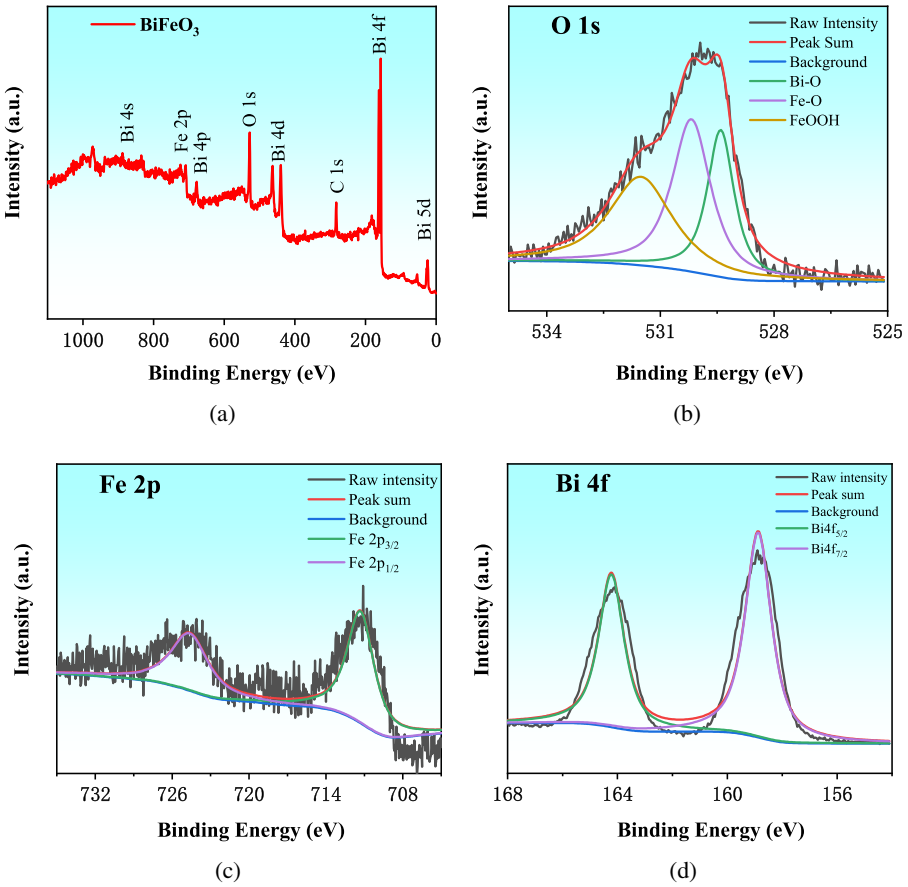

Fig. 6. (a) XPS spectrum of the $BiFeO_3$ precursor synthesized with hydrothermal reaction time of 24 h, (b) O 1*s*, (c) Fe 2*p*, (d) Bi 4*f*.

observed. It can be seen from Fig. 8 that T_C shows an increasing trend, while Tk_ε shows the opposite trend. This indicates that the prolonged reaction time of $BiFeO_3$ precursor enhances the dielectric temperature stability.

3.5. *AC impedance*

Figure 9 shows the Cole–Cole plots of the 0.7BF–0.3BT ceramics at different temperatures. Each sample displays only a single semicircle which indicates the electrical homogeneity resulting from the bulk effect. Therefore, the sample can be considered as a parallel combination of resistance and capacitance. In the case of individual bulk response, the intersection of the low-frequency arc with the Z'-axis can be viewed as the dc resistance of the ceramic. With an increase in temperature, the dc resistance also decreases correspondingly. In Figs. 9(a)–9(d), the radius of the semicircle for each sample decreases with increasing temperature, which means that the impedance decreases with an increase in temperature. This can be explained by the fact that with an increase in temperature, space charge is released and more charge carriers are activated, and therefore, the carrier concentration and mobility increase, leading to a decrease in impedance. By comparing the resistance values of the samples at the same temperature, sample (d) has the largest radius, indicating that it has the highest resistance. This could be due to the longer reaction time of $BiFeO_3$ precursor, which leads to higher crystallinity, larger grain size and uneven grain distribution. The grain size affects the capacitance, which is a contribution to the high-temperature impedance. The ceramic prepared with $BiFeO_3$ precursor with a reaction time of 24 h also has the largest relative dielectric constant, which confirms this phenomenon.

In Figs. 10(a) and 10(b), the frequency dependence of complex impedance (real part Z' and imaginary part Z'') of 0.7BF–0.3BT–4 is shown in the temperature range of 360°C–450°C. From Fig. 10(a), it can be observed that the impedance values show a monotonic decrease with increasing temperature and frequency in the low-frequency range ($\leq$10 kHz). The decrease in Z' with increasing temperature in the low-frequency part indicates an increase in conductivity with temperature. Also, although the Z' value decreases with increasing frequency, it starts to merge at a fixed frequency ($\geq$200 kHz) with increasing frequency. This change represents a possibility of an increase in conductivity with increasing frequency and temperature, because at low temperatures, the charge carriers are fixed, and defects exist at high temperatures. The merging of Z' at high frequencies at all temperatures may be due to the release of space charges, which leads to a decrease in material resistance.

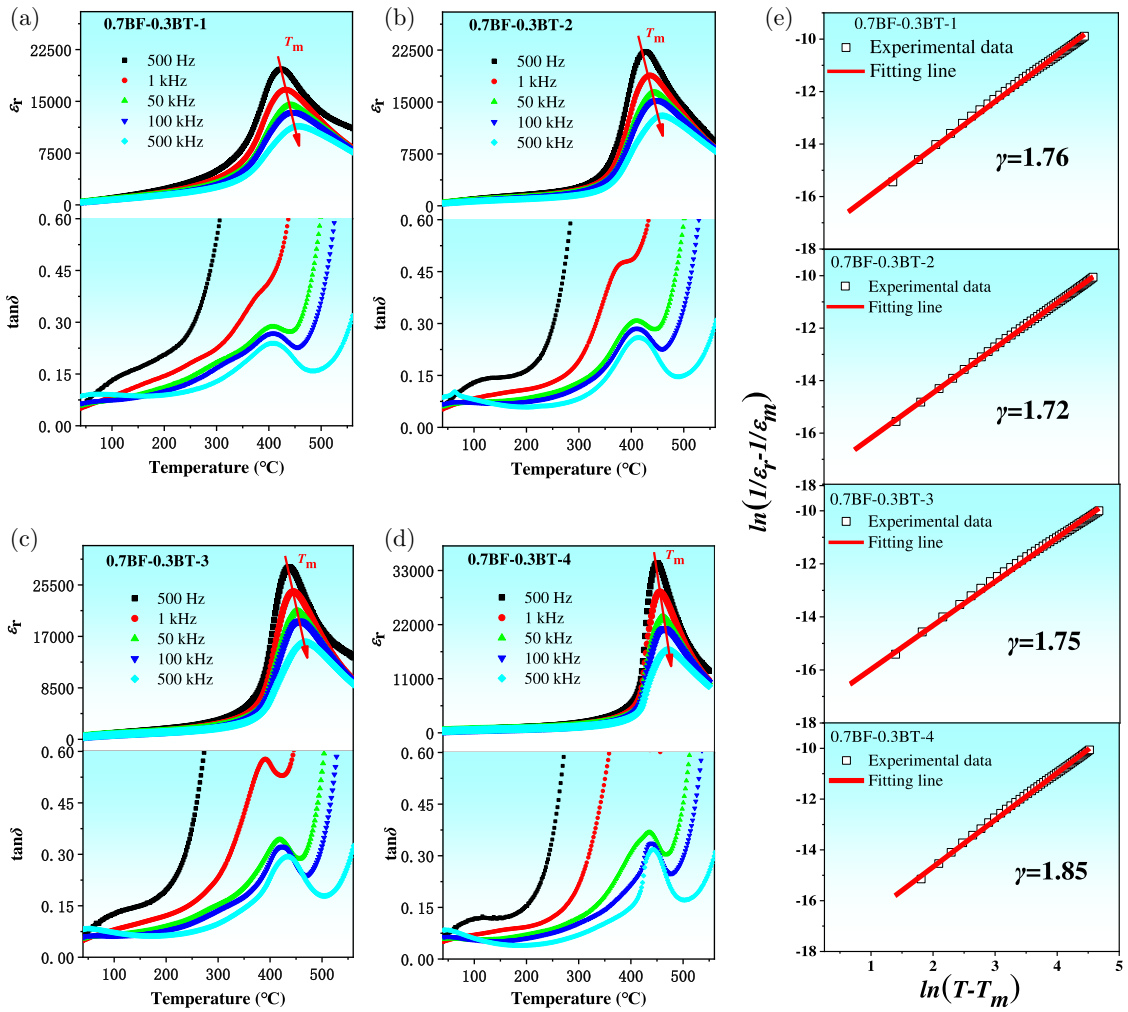

Fig. 7. (a)–(d) Temperature dependence of dielectric properties of the 0.7BF–0.3BT ceramics, (e) the relationship between $\ln(1/\varepsilon_r - 1/\varepsilon_m)$ and $\ln(T - T_m)$ of the 0.7BF–0.3BT ceramics at 100 kHz.

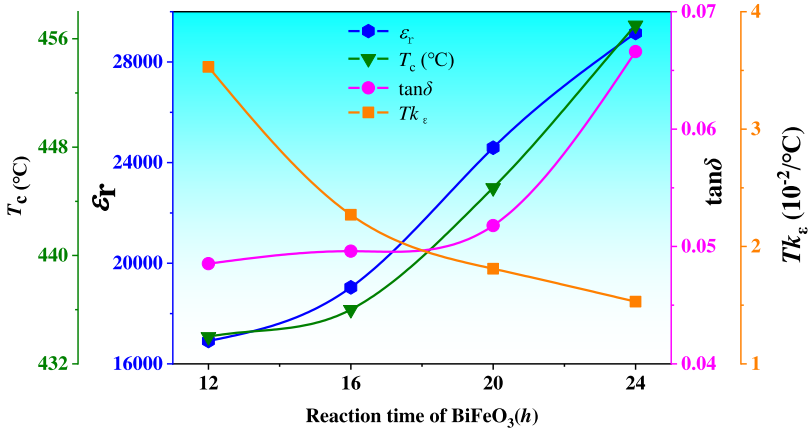

Fig. 8. Dielectric properties of the 0.7BF–0.3BT ceramics as a function of the reaction time of $BiFeO_3$.

From Fig. 10(b), we can see the change of Z'' with frequency at different temperatures. As the temperature increases, all peaks move towards high frequencies and then towards low frequencies, which can be understood as the phase transition and polarization phenomena of BF-BT ceramics. At low temperatures, a narrow imaginary part peak appears at high frequency in BF-BT ceramics, which is caused by transient capacitance and compensating capacitance in the

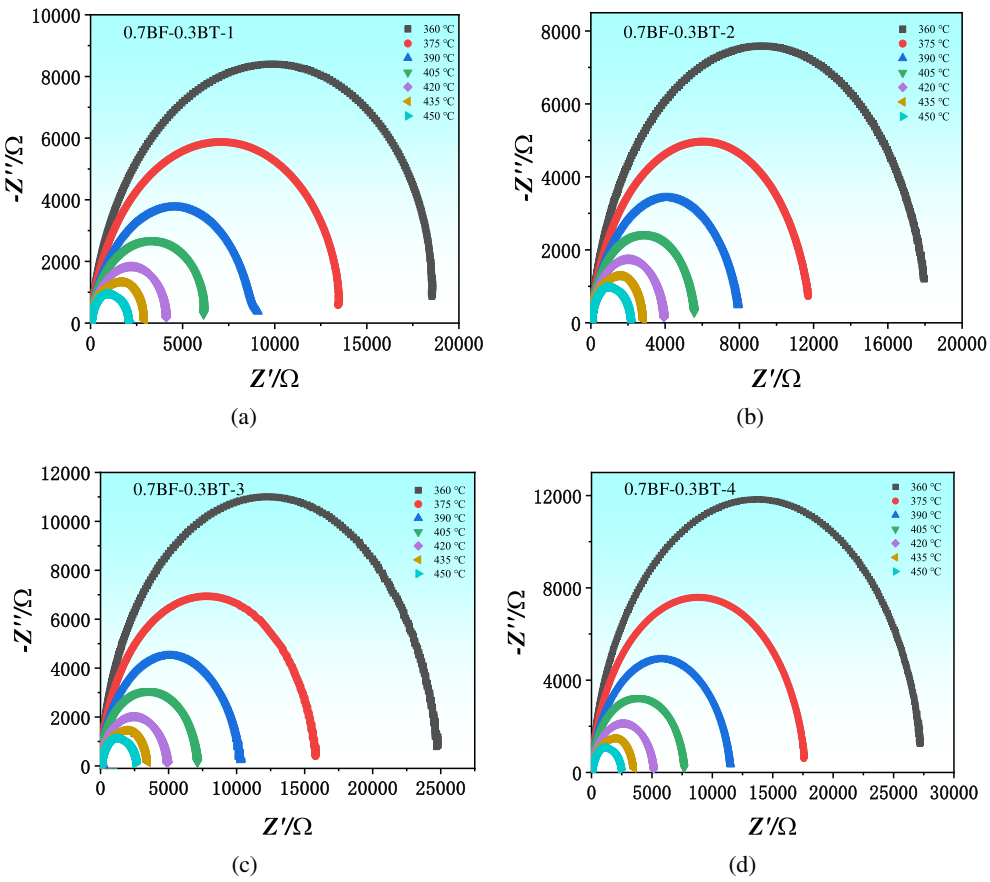

Fig. 9. Cole–Cole plots of the 0.7BF–0.3BT ceramics measured at different temperatures.

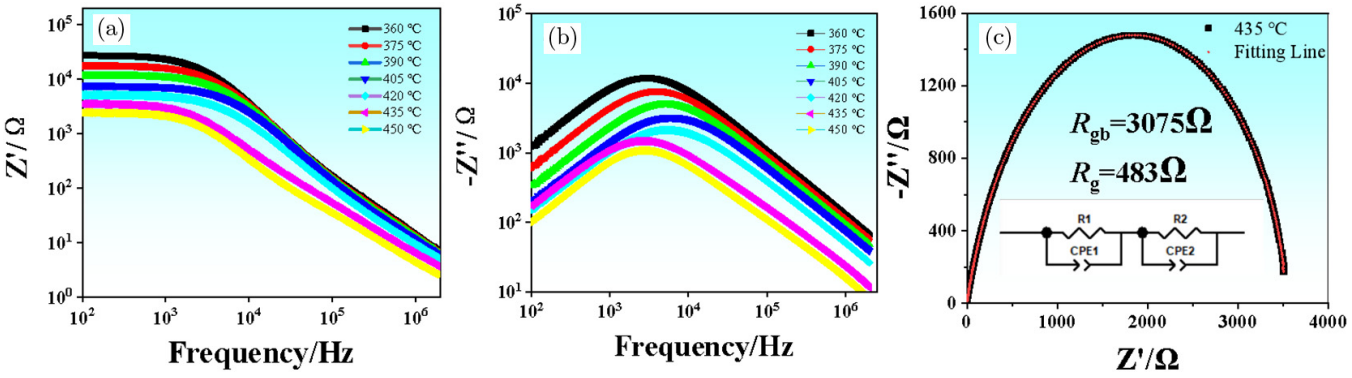

Fig. 10. Frequency dependence of complex impedance spectra of 0.7BF–0.3BT-4, (a) real part (Z'); (b) imaginary part Z'' and (c) equivalent circuit fitting for the Cole–Cole plots.

material. As the temperature increases, this imaginary peak shifts towards high frequencies, which is due to the gradual decrease in the size of ferroelectric domains. Near the phase transition temperature, the ferroelectric-to-paraelectric phase transition occurs in BF-BT ceramics, which leads to the loss of ferroelectric properties and the decrease of surface polarization. This phase transition causes the imaginary part peak to shift towards high frequencies and then towards low frequencies. As the temperature further increases, the imaginary part peak of BF-BT ceramics will continue to shift towards low frequencies, but the intensity of the peak will gradually decrease.

Any nonuniformity in the microstructure will be reflected in the equivalent circuit in the form of a CPE element rather than an ideal capacitor. To obtain the contribution of the grains and grain boundaries of the ceramic in the conductivity process, the complex impedance data of 0.7BF–0.3BT at 435°C was fitted using Z-view software (Fig. 10(c)). Usually,

charge carriers migrate through grains and along grain boundaries, which will result in equivalent resistance and capacitance in grains and grain boundaries. Therefore, the main conduction mechanism is related to the response of ceramic grains and grain boundaries. The low-frequency relaxation is attributed to the contribution of grain boundaries, while the high-frequency relaxation is attributed to grains. To illustrate the contributions of grain boundaries and grains at different stages, the complex impedance data was fitted using*Z*-view software, and the resistance and capacitance of grains and grain boundaries were calculated using the R-CPE equivalent parallel circuit model, as shown in Fig. 10. The fitting results show that the grain boundary resistance ($R_{gb} \approx 3075\ \Omega$) is higher than the grain resistance ($R_g \approx 483\ \Omega$), and the grain boundary mainly hinders the conductivity process at high temperatures.

It can be seen that from Fig. 10(b), $Z''_{\max}$ gradually decreases with increasing temperature, indicating that dielectric behavior exhibits temperature-dependent relaxation phenomena. The relationship between the characteristic frequency f_m corresponding to $Z''_{\max}$ and temperature follows the Arrhenius law below[24]:

$$f_m = f_0 \exp(-E_a^{\text{rel}}/K_B T), \tag{3}$$

where f_m is the characteristic frequency, f_0 is the pre-exponential factor, E_a^{rel} is the relaxation activation energy, K_B is the Boltzmann constant, and T is the thermodynamic temperature (K). According to the formula (3), the relaxation activation energy can be calculated from the Arrenhius plot fitting of the dielectric relaxation data. It can be seen that from the values in Fig. 11, as the reaction time of $BiFeO_3$ precursor increases, E_a^{rel} gradually increases. This may be because prolonging the reaction time of $BiFeO_3$ precursor can make the BF particles smaller and promote even distribution of the particles, leading to better crystallization of the 0.7BF–0.3BT ceramics, smaller grain sizes, and increased numbers of grain boundaries, which in turn leads the relaxation activation energy of ceramics to gradually increase.

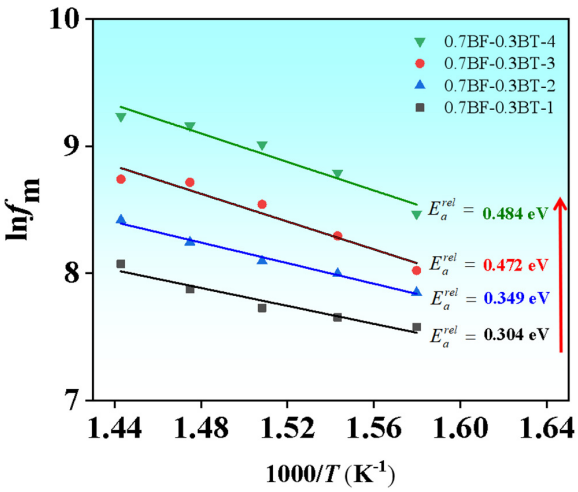

Fig. 11. Arrenhius plot fitting of the dielectric relaxation data of the 0.7BF–0.3BT ceramics.

4. Conclusions

In this study, both $BiFeO_3$ and $BaTiO_3$ powders were prepared by a hydrothermal method and then they were used as precursors for preparing the $0.7BiFeO_3$–$0.3BaTiO_3$ piezoceramics through a pressureless sintering process. The influence of the hydrothermal reaction time of $BiFeO_3$ precursor on the structures, dielectric properties and AC impedance characteristics of the $0.7BiFeO_3$–$0.3BaTiO_3$ ceramics were investigated. The main conclusions are as follows:

(1) All the samples were identified with a coexistence of trigonal and tetragonal phases, with increasing the hydrothermal reaction time of $BiFeO_3$ precursor, the content of the tetragonal phase in the samples gradually increases.
(2) All the samples exhibited a homogeneous grain distribution in the prepared ceramics. As the hydrothermal reaction time of $BiFeO_3$ precursor increases, the grains of the ceramics grew gradually and become more and more rounded. XPS analysis confirmed the presence of Fe^{3+} oxidation state in the prepared $BiFeO_3$ sample.
(3) The 0.7BF–0.3BT ceramics exhibited the notable dielectric relaxor behavior. Both ε_r and T_C of the $0.7BiFeO_3$–$0.3BaTiO_3$ ceramics increased with increasing the hydrothermal reaction time of $BiFeO_3$, while Tk_ε decreases with it. 0.7BF–0.3BT-4 possesses a higher $\tan\delta$ than other samples.
(4) 0.7BF–0.3BT-4 was also found with a higher AC impedance than others, and the calculation based on the R-CPE circuit model showed that the grain boundary resistance of the ceramic had a greater contribution to its conduction mechanism at high temperatures.

Acknowledgments

This work was funded by the Guangdong Provincial Key Laboratory of Materials and Technologies for Energy Conversion (No. MATEC2022KF001), as well as the project for cultivating High-level Talents and National Natural Science Foundation at the Chengdu University (No. Z1350).

ORCID

Shuangchi Li https://orcid.org/0009-0009-2010-3801
Fang Wang https://orcid.org/0009-0008-4086-1653
Lanxin Tang https://orcid.org/0009-0007-3948-2157
Daniel Q. Tan https://orcid.org/0000-0002-2282-2000
Yu Chen https://orcid.org/0000-0001-6707-7182

References

[1]Y. Chen, H. Fan, D. Hou, Y. Jia, A. Zhang and W. Wang, Bismuth sodium titanate–barium titanate–barium zirconate titanate relaxor

ferroelectric ceramics with high recoverable energy storage density, *Ceram. Int.* **48**(18), 26894 (2022).
[2]M. Chen, Y. Jia, H. Li, Z. Wu, T. Huang and H. Zhang, Enhanced pyrocatalysis of the pyroelectric $BiFeO_3$/g-C_3N_4 heterostructure for dye decomposition driven by cold-hot temperature alternation, *J. Adv. Ceram.* **10**(2), 339 (2021).
[3]C. Yu, M. Tan, C. Tao, Y. Hou, C. Liu, H. Meng, Y. Su, L. Qiao and Y. Bai, Remarkably enhanced piezo-photocatalytic performance in $BaTiO_3$/CuO heterostructures for organic pollutant degradation, *J. Adv. Ceram.* **11**(3), 415 (2022).
[4]Y. Wan, Y. Li, Q. Li, W. Zhou, Q. Zheng, X. Wu, C. Xu, B. Zhu, D. Lin and J. Jones, Microstructure, ferroelectric, piezoelectric, and ferromagnetic properties of Sc-modified $BiFeO_3$–$BaTiO_3$ multiferroic ceramics with MnO_2 addition, *J. Am. Ceram. Soc.* **97**(6), 1809 (2014).
[5]N. Setter and L. E. Cross, The role of *B*-site cation disorder in diffuse phase transition behavior of perovskite ferroelectrics, *J. Appl. Phys.* **51**(8), 4356 (2008).
[6]T. Gao, Z. Chen, F. Niu, D. Zhou, Q. Huang, Y. Zhu, L. Qin, X. Sun and Y. Huang, Shape-controlled preparation of bismuth ferrite by hydrothermal method and their visible-light degradation properties, *J. Alloys Compd.* **648**, 564 (2015).
[7]D. C. Gonmei and I. Soibam, Soaking time effect on the properties of perovskite structure bismuth ferrite, *Indian J. Phys.* 1 (2023).
[8]T. Cui, J. Zhang, J. Guo, X. Li, S. Guo, Y. Huan, J. Wang, S.-T. Zhang and Y. Wang, Outstanding comprehensive energy storage performance in lead-free $BiFeO_3$-based relaxor ferroelectric ceramics by multiple optimization design, *Acta Mater.* **240**, 2 (2022).
[9]H. Bai, J. Li, Y. Hong and Z. Zhou, Enhanced ferroelectricity and magnetism of quenched $(1-x)BiFeO_3-xBaTiO_3$ ceramics, *J.dv. Ceram.* **9**(4), 511 (2020).
[10]A. Prasatkhetragarn, P. Muangkonkad, P. Aommongkol, P. Jantaratana, N. Vittayakorn and R. Yimnirun, Investigation on ferromagnetic and ferroelectric properties of (La, K)-doped $BiFeO_3$–$BaTiO_3$ solid solution, *Ceram. Int.* **39**, 249 (2013).
[11]Y. Cui, X. Zhang, X. Lei, T. Yan, X. Chen, B. Peng, P. Ren, C. Li and L. Liu, The high piezoelectricity and thermal stability of high-temperature piezoelectric ceramics $BiFeO_3$–$0.25BaTiO_3$–$xBi_{0.5}K_{0.5}TiO_3$ near the MPB, *J. Mater. Chem. C* **10**(21), 8302 (2022).
[12]V. Purohit and R. N. P. Choudhary, Structural, microstructural and electrical properties of $BiFeO_3$ and $BaTiO_3$ modified Bi $(Ca_{0.5}Ti_{0.5})O_3$ perovskite, *J. Solid State Chem.* **292**, 2 (2020).
[13]Y. Yan, X. Zeng, M. Tang, S. Song, F. Chen, Y. Wang, L. Yang, L. Jin and G. Liu, Enhancement in energy storage performance of La-modified bismuth–ferrite-based relaxor ferroelectric ceramics by defect compensation and process optimization, *Ceram. Int.* **48**(22), 33554 (2022).
[14]O. Tokay and M. Yazıcı, A review of potassium sodium niobate and bismuth sodium titanate based lead free piezoceramics, *Mater. Today Commun.* **31**(12), 9092 (2022).
[15]S. Cheng, B.-P. Zhang, L. Zhao and K.-K. Wang, Enhanced insulating and piezoelectric properties of $0.7BiFeO_3$–$0.3BaTiO_3$ lead-free ceramics by optimizing calcination temperature: analysis of Bi_{3+} volatilization and phase structures, *J. Mater. Chem. C* **6**(15), 3982 (2018).
[16]B.-W. Xun, N. Wang, B.-P. Zhang, X.-Y. Chen, Y.-Q. Zheng, W.-S. Jin, R. Mao and K. Liang, Enhanced piezoelectric properties of $_{0.7}BiFeO_3$–$_{0.3}BaTiO_3$ lead-free piezoceramics with high Curie temperature by optimizing Bi self-compensation, *Ceram. Int.* **45**(18), 2 (2019).
[17]S. Cheng, L. Zhao, B.-P. Zhang and K.-K. Wang, Lead-free $0.7BiFeO_3$–$0.3BaTiO_3$ high-temperature piezoelectric ceramics: Nano-$BaTiO_3$ raw powder leading to a distinct reaction path and enhanced electrical properties, *Ceram. Int.* **45**(8), 4 (2019).
[18]H. Wang, P. Zhao, L. Chen, L. Li and X. Wang, Energy storage properties of $0.87BaTiO_3-_{0.13}Bi(Zn_2/_3(Nb_{0.85}Ta_{0.15})1/3)O_3$ multilayer ceramic capacitors with thin dielectric layers, *J. Adv. Ceram.* **9**(3), 293 (2020).
[19]S. L. Rasheed and E. K. Al-Shakarchi, The nanostructure of barium dititanate prepared by hydrothermal method, *J. Adv. Dielectr.* **9**(2), 1 (2019).
[20]N. Ma, B.-P. Zhang, W.-G. Yang and D. Guo, Phase structure and nano-domain in high performance of BaTiO3 piezoelectric ceramics, *J. Eur. Ceram. Soc.* **32**(5), 1059 (2012).
[21]L.-F. Zhu, B.-P. Zhang, Z.-C. Zhang, S. Li, L.-J. Wang and L.-J. Zheng, Piezoelectric, ferroelectric and ferromagnetic properties of $(1-x)BiFeO_3$–$xBaTiO_3$ lead-free ceramics near morphotropic phase boundary, *J. Mater. Sci.: Mater. Electron.* **29**(3), 1 (2017).
[22]S. O. Leontsev and R. E. Eitel, Dielectric and piezoelectric properties in Mn-modified (1–x)$BiFeO_3$–x$BaTiO_3$ ceramics, *J. Am. Ceram. Soc.* **92**(12), 2958 (2009).
[23]Q. Zhou, C. Zhou, H. Yang, G. Chen, W. Li, H. Wang and S. Zhang, Dielectric, ferroelectric, and piezoelectric properties of $Bi(Ni_{1/2}Ti_{1/2})O_3$-Modified $BiFeO_3$–$BaTiO_3$ ceramics with high Curie temperature, *J. Am. Ceram. Soc.* **95**(12), 3892 (2012).
[24]S. Cheng, B.-P. Zhang, L. Zhao and K.-K. Wang, Enhanced insulating and piezoelectric properties of $BiFeO_3$–$BaTiO_3$–$Bi_{0.5}Na_{0.5}TiO_3$ ceramics with high Curie temperature, *J. Am. Ceram. Soc.* **102**, 7356 (2019).
[25]H. Qin, J. Zhao, X. Chen, H. Li, S. Wang, Y. Du, P. Li, H. Zhou and D. Wang, Investigation of lead-free $BiFeO_3$–$BaTiO_3$ piezoelectric ceramics through precise composition control, *J. Adv. Dielectr.* **13**, 2350018 (2023).
[26]D. J. Dmonte, A. Bhardwaj, M. Wilhelm, T. Fischer, I. Kuritka and S. Mathur, Sub PPM detection of $NO_{(2)}$ using strontium doped bismuth ferrite nanostructures, *Micromachines (Basel)* **14**(3), 7 (2023).
[27]Z. Mou, R. Yan, J. Peng, Y. Li, Z. Huang, Z. Wang, B. Zhao and D. Xiao, Synthesis of polyzwitterionic carbon dots with superior friction and fatigue control behaviors under water lubrication, *Chem. Eng. J.* **465**, 4 (2023).
[28]N. Panda, S. Pattanayak, R. N. P. Choudhary and A. Kumar, Retracted article: Effect of La-substitution on structural, dielectric and electrical properties of $(Bi_{0.5}Pb_{0.5})$ $(Fe_{0.5}Zr_{0.25}Ti_{0.25})O_3$, *Appl. Phys. A* **122**(9), 2 (2016).
[29]Z. Mou, J. Peng, R. Yan, Q. Yang, B. Zhao and D. Xiao, Electrical stimulation enables dynamic regulation of the tribological behaviors of polyelectrolyte-modified carbon dots, *Carbon* **203**, 17 (2023).
[30]K. Idczak and R. Idczak, Investigation of surface segregation in Fe-Cr-Si alloys by XPS, *Metall. Mater Trans A* **51**(6), 3078 (2020).
[31]Y. Chen, S. Xie, H. Wang, Q. Chen, Q. Wang, J. Zhu and Z. Guan, Dielectric abnormality and ferroelectric asymmetry in W/Cr co-doped $Bi_4Ti_3O_{12}$ ceramics based on the effect of defect dipoles, *J. Alloys Compd.* **696**, 750 (2017).